

Three flavor neutrino oscillation analysis of atmospheric neutrinos in Super-Kamiokande

J.Hosaka,¹ K.Ishihara,¹ J.Kameda,¹ Y.Koshio,¹ A.Minamino,¹ C.Mitsuda,¹ M.Miura,¹ S.Moriyama,¹ M.Nakahata,¹ T.Namba,¹ Y.Obayashi,¹ M.Shiozawa,¹ Y.Suzuki,¹ A.Takeda,¹ Y.Takeuchi,¹ S.Yamada,¹ I.Higuchi,² M.Ishitsuka,² T.Kajita,² K.Kaneyuki,² G.Mitsuka,² S.Nakayama,² H.Nishino,² A.Okada,² K.Okumura,² C.Saji,² Y.Takenaga,² S.Clark,³ S.Desai,^{3,*} E.Kearns,³ S.Likhoded,³ J.L.Stone,³ L.R.Sulak,³ W.Wang,³ M.Goldhaber,⁴ D.Casper,⁵ J.P.Cravens,⁵ W.R.Kropp,⁵ D.W.Liu,⁵ S.Mine,⁵ C.Regis,⁵ M.B.Smy,⁵ H.W.Sobel,⁵ C.W.Sterner,⁵ M.R.Vagins,⁵ K.S.Ganezer,⁶ J.E.Hill,⁶ W.E.Keig,⁶ J.S.Jang,⁷ J.Y.Kim,⁷ I.T.Lim,⁷ K.Scholberg,⁸ C.W.Walter,⁸ R.W.Ellsworth,⁹ S.Tasaka,¹⁰ E.Guillian,¹¹ A.Kibayashi,¹¹ J.G.Learned,¹¹ S.Matsuno,¹¹ M.D.Messier,¹² Y.Hayato,^{13,†} A.K.Ichikawa,¹³ T.Ishida,¹³ T.Ishii,¹³ T.Iwashita,¹³ T.Kobayashi,¹³ T.Nakadaira,¹³ K.Nakamura,¹³ K.Nitta,¹³ Y.Oyama,¹³ Y.Totsuka,¹³ A.T.Suzuki,¹⁴ M.Hasegawa,¹⁵ I.Kato,^{15,‡} H.Maesaka,¹⁵ T.Nakaya,¹⁵ K.Nishikawa,¹⁵ T.Sasaki,¹⁵ H.Sato,¹⁵ S.Yamamoto,¹⁵ M.Yokoyama,¹⁵ T.J.Haines,^{16,5} S.Dazeley,¹⁷ S.Hatakeyama,¹⁷ R.Svoboda,¹⁷ E.Blaufuss,¹⁸ J.A.Goodman,¹⁸ G.W.Sullivan,¹⁸ D.Turcan,¹⁸ J.Cooley,¹⁹ A.Habig,²⁰ Y.Fukuda,²¹ T.Sato,²¹ Y.Itow,²² C.K.Jung,²³ T.Kato,²³ K.Kobayashi,²³ M.Malek,²³ C.Mauger,²³ C.McGrew,²³ A.Sarrat,^{1,23} C.Yanagisawa,²³ N.Tamura,²⁴ M.Sakuda,²⁵ Y.Kuno,²⁶ M.Yoshida,²⁶ S.B.Kim,²⁷ J.Yoo,²⁷ T.Ishizuka,²⁸ H.Okazawa,²⁹ Y.Choi,³⁰ H.K.Seo,³⁰ Y.Gando,³¹ T.Hasegawa,³¹ K.Inoue,³¹ J.Shirai,³¹ A.Suzuki,³¹ K.Nishijima,³² H.Ishino,³³ Y.Watanabe,³³ M.Koshiba,³⁴ D.Kielczewska,^{35,5} J.Zalipska,³⁵ H.G.Berns,³⁶ R.Gran,^{36,20} K.K.Shiraishi,³⁶ A.Stachyra,³⁶ K.Washburn,³⁶ and R.J.Wilkes³⁶

(The Super-Kamiokande Collaboration)

¹Kamioka Observatory, Institute for Cosmic Ray Research, University of Tokyo, Kamioka, Gifu, 506-1205, Japan

²Research Center for Cosmic Neutrinos, Institute for Cosmic Ray Research, University of Tokyo, Kashiwa, Chiba 277-8582, Japan

³Department of Physics, Boston University, Boston, MA 02215, USA

⁴Physics Department, Brookhaven National Laboratory, Upton, NY 11973, USA

⁵Department of Physics and Astronomy, University of California, Irvine, Irvine, CA 92697-4575, USA

⁶Department of Physics, California State University, Dominguez Hills, Carson, CA 90747, USA

⁷Department of Physics, Chonnam National University, Kwangju 500-757, Korea

⁸Department of Physics, Duke University, Durham, NC 27708 USA

⁹Department of Physics, George Mason University, Fairfax, VA 22030, USA

¹⁰Department of Physics, Gifu University, Gifu, Gifu 501-1193, Japan

¹¹Department of Physics and Astronomy, University of Hawaii, Honolulu, HI 96822, USA

¹²Department of Physics, Indiana University, Bloomington, IN 47405-7105, USA

¹³High Energy Accelerator Research Organization (KEK), Tsukuba, Ibaraki 305-0801, Japan

¹⁴Department of Physics, Kobe University, Kobe, Hyogo 657-8501, Japan

¹⁵Department of Physics, Kyoto University, Kyoto 606-8502, Japan

¹⁶Physics Division, P-23, Los Alamos National Laboratory, Los Alamos, NM 87544, USA

¹⁷Department of Physics and Astronomy, Louisiana State University, Baton Rouge, LA 70803, USA

¹⁸Department of Physics, University of Maryland, College Park, MD 20742, USA

¹⁹Department of Physics, Massachusetts Institute of Technology, Cambridge, MA 02139, USA

²⁰Department of Physics, University of Minnesota, Duluth, MN 55812-2496, USA

²¹Department of Physics, Miyagi University of Education, Sendai, Miyagi 980-0845, Japan

²²Solar-Terrestrial Environment Laboratory, Nagoya University, Nagoya, Aichi 464-8601, Japan

²³Department of Physics and Astronomy, State University of New York, Stony Brook, NY 11794-3800, USA

²⁴Department of Physics, Niigata University, Niigata, Niigata 950-2181, Japan

²⁵Department of Physics, Okayama University, Okayama, Okayama 700-8530, Japan

²⁶Department of Physics, Osaka University, Toyonaka, Osaka 560-0043, Japan

²⁷Department of Physics, Seoul National University, Seoul 151-742, Korea

²⁸Department of Systems Engineering, Shizuoka University, Hamamatsu, Shizuoka 432-8561, Japan

²⁹Department of Informatics in Social Welfare, Shizuoka University of Welfare, Yaizu, Shizuoka 425-8611, Japan

³⁰Department of Physics, Sungkyunkwan University, Suwon 440-746, Korea

³¹Research Center for Neutrino Science, Tohoku University, Sendai, Miyagi 980-8578, Japan

³²Department of Physics, Tokai University, Hiratsuka, Kanagawa 259-1292, Japan

³³Department of Physics, Tokyo Institute for Technology, Meguro, Tokyo 152-8551, Japan

³⁴University of Tokyo, Tokyo 113-0033, Japan

³⁵Institute of Experimental Physics, Warsaw University, 00-681 Warsaw, Poland

³⁶Department of Physics, University of Washington, Seattle, WA 98195-1560, USA

(Dated: May 25, 2019)

We report on the results of a three-flavor oscillation analysis using Super-Kamiokande I atmospheric neutrino data, with the assumption of one mass scale dominance ($\Delta m_{12}^2=0$). No significant flux change due to matter effect, which occurs when neutrinos propagate inside the Earth for $\theta_{13}\neq 0$, has been seen either in a multi-GeV ν_e -rich sample or in a ν_μ -rich sample. A constraint on θ_{13} is given using Super-Kamiokande data only. Both normal and inverted mass hierarchy hypotheses are tested and both are consistent with observation.

PACS numbers: 14.60.Pq, 96.50.S-

I. INTRODUCTION

Recently a number of experiments have shown evidence for oscillations of atmospheric [1, 2, 3, 4, 5, 6], solar [7, 8], reactor [9], and accelerator neutrinos [10].

In the standard oscillation picture, the three neutrino flavor eigenstates are related to the mass eigenstates by a 3×3 unitary mixing matrix U :

$$|\nu_\alpha\rangle = \sum_{i=1}^3 U_{\alpha i} |\nu_i\rangle. \quad (1)$$

In this picture, neutrino oscillations can be described by six parameters: two independent Δm_{ij}^2 ($\Delta m_{12}^2, \Delta m_{23}^2$), three mixing angles ($\theta_{12}, \theta_{23}, \theta_{13}$), and a CP-violating phase δ . The mixing matrix U of Eq. 1 can be written as a product of three rotations, each described by one of the mixing angles:

$$U = \begin{pmatrix} 1 & 0 & 0 \\ 0 & c_{23} & s_{23} \\ 0 & -s_{23} & c_{23} \end{pmatrix} \begin{pmatrix} c_{13} & 0 & s_{13}e^{-i\delta} \\ 0 & 1 & 0 \\ -s_{13}e^{i\delta} & 0 & c_{13} \end{pmatrix} \times \begin{pmatrix} c_{12} & s_{12} & 0 \\ -s_{12} & c_{12} & 0 \\ 0 & 0 & 1 \end{pmatrix} \quad (2)$$

where “s” represents sine of the mixing angle and “c” represents cosine.

The “1-2” matrix describes solar mixing; the “2-3” matrix describes atmospheric neutrino mixing. The “1-3” mixing is known to be small; the best current limits on θ_{13} come from the CHOOZ experiment [11].

As yet, the Super-Kamiokande atmospheric neutrino oscillation fits have been done within a two-flavor oscillation framework [5, 12]. In this paper, we explore the atmospheric data in the context of a three-flavor analysis.

Among the remaining problems in neutrino physics that can be answered by oscillation experiments are whether θ_{13} is non-zero, and whether the hierarchy is normal or inverted, *i.e.* whether Δm_{23}^2 is positive or

negative. At baselines and energies appropriate for atmospheric neutrinos, the signature of a non-zero θ_{13} is a matter-enhanced excess of upward-going electron-like events. One can, in principle, distinguish between inverted and normal hierarchy by comparing the behavior of neutrinos and anti-neutrinos in matter. In a detector such as Super-K, one cannot distinguish between ν and $\bar{\nu}$ on an event-by-event basis. However, due to a difference in both total and differential interaction cross-section between neutrinos and anti-neutrinos, one can gain information statistically about the hierarchy using atmospheric neutrinos.

II. THREE NEUTRINO OSCILLATION WITH ONE MASS SCALE DOMINANT

In general, neutrino oscillations are driven by differences of squared masses, m_1^2, m_2^2, m_3^2 . We have adopted the so-called “one mass scale dominance” framework:

$$|m_2^2 - m_1^2| \ll |m_3^2 - m_{1,2}^2| \quad (3)$$

This approximation is supported by experimental observations of solar, reactor, atmospheric and accelerator neutrino oscillations. The advantage of this framework is that the number of parameters involved in neutrino oscillations is reduced to three: two mixing angles (θ_{23}, θ_{13}) and one mass squared difference Δm^2 ,

$$\Delta m^2 \equiv m_3^2 - m_{1,2}^2. \quad (4)$$

The ignored oscillation effects driven by the smaller mass difference $\Delta m_{12}^2 \equiv |m_2^2 - m_1^2|$, which might be observed for a neutrino energy of a few hundred MeV, are known to be greatly reduced in the case that the initial flavor flux ratio of ν_μ/ν_e is 2 and $\sin^2 2\theta_{23}$ is close to one [13]. Equation 3 can hold both for $m_{1,2}^2 \ll m_3^2$ (normal mass hierarchy) and $m_3^2 \ll m_{1,2}^2$ (inverted mass hierarchy). We present tests of both cases in this paper.

In this framework, in the case of non-zero θ_{13} the neutrino transition and survival probabilities in vacuum, valid for down-going atmospheric neutrinos, are

*Present address: Center for Gravitational Wave Physics, Pennsylvania State University, University Park, PA 16802, USA

†Present address: Kamioka Observatory, Institute for Cosmic Ray Research, University of Tokyo, Kamioka, Gifu, 506-1205, Japan

‡Present address: TRIUMF, Vancouver, British Columbia V6T 2A3, Canada

expressed as

$$\begin{aligned}
P(\nu_e \rightarrow \nu_e) &= 1 - \sin^2 2\theta_{13} \sin^2\left(\frac{1.27\Delta m^2 L}{E}\right) \\
P(\nu_\mu \rightarrow \nu_e) &= P(\nu_e \rightarrow \nu_\mu) \\
&= \sin^2 \theta_{23} \sin^2 2\theta_{13} \sin^2\left(\frac{1.27\Delta m^2 L}{E}\right) \\
P(\nu_\mu \rightarrow \nu_\mu) &= 1 \\
&\quad - 4 \cos^2 \theta_{13} \sin^2 \theta_{23} (1 - \cos^2 \theta_{13} \sin^2 \theta_{23}) \\
&\quad \times \sin^2\left(\frac{1.27\Delta m^2 L}{E}\right) \quad (5)
\end{aligned}$$

where L is neutrino travel length from the neutrino production point in the atmosphere and E is neutrino energy. In the limit of zero θ_{13} , these equations reduce to pure $\nu_\mu \leftrightarrow \nu_\tau$ 2-flavor oscillation. Because $P(\nu_e \rightarrow \nu_e)$ in Eq. 5 is a function of $\sin^2 2\theta_{13}$, both $\sin^2 \theta_{13} \sim 0$ and $\sin^2 \theta_{13} \sim 1$ can satisfy $P(\nu_e \rightarrow \nu_e) \sim 1$ observed by reactor neutrino experiments. However, $\sin^2 \theta_{13} \sim 1$ is inconsistent with an observed large deficit of atmospheric ν_μ because $P(\nu_\mu \rightarrow \nu_\mu)$ in Eq. 5 becomes ~ 1 for this case. Therefore, $\sin^2 \theta_{13} > 0.5$ is not discussed here.

Oscillation probability is calculated taking into account Earth's matter potential for neutrinos traversing the Earth [14, 15, 16]. We adopted a model in which the Earth is well-approximated by four layers of a constant matter density (core 1: $R \leq 1221$ km, $\rho = 13.0$ g/cm³, core 2: $1221 < R \leq 3480$ km, $\rho = 11.3$ g/cm³, mantle: $3480 < R \leq 5701$ km, $\rho = 5.0$ g/cm³, surface: $5701 < R \leq 6371$ km, $\rho = 3.3$ g/cm³). The method of calculating matter oscillation probabilities in constant density is based on [17].

Due to the matter effect, the $\nu_\mu \rightarrow \nu_e$ oscillation probability becomes large at 5 ~ 10 GeV neutrino energy even for the case of small θ_{13} [18, 19, 20, 21]. To demonstrate the behavior of ν_e oscillations, Fig. 1 shows the transition probability of ν_e to ν_μ after traversing the Earth. Note that for normal mass hierarchy, the ν_e flux is resonantly enhanced, and there is no enhancement for anti-neutrinos; the situation is reversed for the inverted mass hierarchy. Also note that net appearance of ν_e (or $\bar{\nu}_e$) is smaller than this transition probability, because ν_e disappearance compensates for some $\nu_\mu \rightarrow \nu_e$. The signature of non-zero θ_{13} corresponds to a small net enhancement of ν_e (or $\bar{\nu}_e$) in the resonance region, as well as a small deficit of ν_μ with respect to two-flavor $\nu_\mu \rightarrow \nu_\tau$ oscillations. In matter, the solar and the interference terms modify the ν_e enhancement in the resonance region by less than 5%, justifying our assumption of $\Delta m_{12}^2 = 0$.

In order to minimize the effect of insufficient statistics of Monte Carlo events, probabilities are averaged out with regard to oscillation phase when a neutrino propagates more than two times the oscillation wavelength in the last part of Earth's mantle in its trajectory.

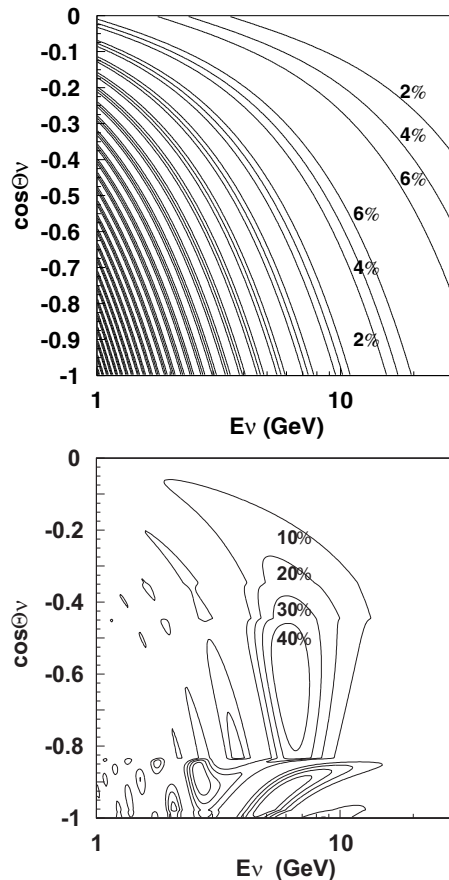


FIG. 1: Oscillation probability of $\nu_e \rightarrow \nu_\mu$ transition. For both figures, the horizontal axis shows neutrino energy and the vertical axis shows the zenith angle of neutrino direction; $\cos \Theta_\nu = -1$ and $\cos \Theta_\nu = 0$ correspond to vertically upward and horizontal directions, respectively. Assumed oscillation parameters are ($\Delta m^2 = 2.5 \times 10^{-3} \text{ eV}^2$, $\sin^2 \theta_{23} = 0.5$, $\sin^2 \theta_{13} = 0.04$.) The top figure assumes neutrino oscillation in vacuum and the bottom figure takes into account Earth's matter effect.

III. DATA SAMPLE

Super-Kamiokande is a 22.5kt fiducial mass water Cherenkov detector located at a depth of 2700m water equivalent in the Kamioka mine, Gifu, Japan. The detector is optically separated into two concentric cylindrical regions. The inner detector (ID) is instrumented with 11,146 20-inch photomultiplier tubes (PMT). The outer detector is instrumented with 1,885 8-inch PMTs. Details of the detector can be found in Ref. [22]. Physical quantities associated with a neutrino event such as the interaction vertex, the number of Cherenkov rings, the direction of each ring, particle identification (PID), momentum, and number of Michel electrons are reconstructed by using hit timing and charge distributions of Cherenkov ring images recorded by PMTs on the ID wall.

Atmospheric neutrino data are categorized into fully-

contained (FC), partially-contained (PC), and upward-going muons (UP μ). FC events deposit all of their Cherenkov light inside the ID. PC events have an exiting particle that deposits visible energy in the OD. UP μ events are neutrino interactions in the rock below the detector for which muons either stop in the detector, or pass through the detector. In the present analysis, we use 1489 live-days of FC, PC and 1646 days UP μ neutrino data taken from May 1996 through July 2001 during the Super-Kamiokande I period.

The FC sample is divided into sub-GeV and multi-GeV subsamples according to the visible energy as $E_{vis} < 1.33$ GeV for sub-GeV, $E_{vis} > 1.33$ GeV for multi-GeV where the visible energy of an event is the total energy assuming all Cherenkov light is from electromagnetic showers. The sample is also divided into single-ring and multi-ring by number of reconstructed Cherenkov rings, and into e -like and μ -like by PID of the most energetic ring. Sub- and multi-GeV, e - and μ -like events from the single-ring sample, and sub- and multi-GeV μ -like events from the multi-ring sample are used in the analysis, as for the $\nu_\mu \rightarrow \nu_\tau$ 2-flavor oscillation analysis [5]. The PC sample is divided into ‘OD stopping events’ and ‘OD through-going events’ according to energy deposited in the OD [12]. The UP μ sample is divided into upward stopping muons (entering and stopping in the tank) and upward through-going muons (passing through the tank).

As mentioned in the previous section, an excess of upward-going ν_e and/or $\bar{\nu}_e$ in the few-GeV region is expected for certain oscillation parameter sets. To improve the sensitivity to this case, a ν_e -enriched sample is selected from the multi-GeV multi-ring e -like sample and is used in addition to the standard oscillation analysis samples. The ν_e -enriched selection is based on a likelihood analysis using PID likelihood, momentum fraction of the most energetic ring, number of muon decay electrons, and distance between muon decay electron and primary neutrino interaction position. Figure 2 shows distributions used to obtain the ν_e -enriched likelihood function. $\nu_e + \bar{\nu}_e$ charged current (CC) and ν_μ CC + $\bar{\nu}_\mu$ CC + neutral current (NC) interactions are separately shown. As is shown in Table I, the $\nu_e + \bar{\nu}_e$ fraction

TABLE I: Breakdown of multi-GeV multi-ring e -like events in the MC sample before and after a ν_e -enrichment based on a likelihood analysis. For each interaction mode, the number of events normalized to 1489 live-days and the fraction are shown assuming pure $\nu_\mu \leftrightarrow \nu_\tau$ 2-flavor oscillation ($\Delta m^2 = 2.5 \times 10^{-3} \text{eV}^2$, $\sin^2 \theta_{23} = 0.5$, $\sin^2 \theta_{13} = 0$). Survival efficiency for $\nu_e + \bar{\nu}_e$ CC events is 66.8%.

multi-GeV multi-ring e -like events	$\nu_e + \bar{\nu}_e$ CC	$\nu_\mu + \bar{\nu}_\mu$ CC	NC	total
no likelihood cut	630.8 55.8%	242.2 21.4%	258.0 22.8%	1131.1 100%
likelihood cut	421.3 75.6%	49.1 8.8%	86.8 15.6%	557.3 100%
efficiency	66.8%			

in the multi-GeV multi-ring e -like sample is improved to 75.6% after the likelihood cut. A summary of the number of observed and expected FC multi-ring e -like events is shown in Table III in the appendix.

IV. OSCILLATION ANALYSIS

The oscillation analysis is performed by comparing data with MC equivalent to 100 years of detector exposure. The atmospheric neutrino flux calculation from [23] and neutrino interaction model (NEUT) [5, 24] are used to simulate interactions with the nuclei of water, or in the case of upward muons, the nuclei of the rock surrounding the detector. A GEANT-based full detector simulation is used to generate the MC neutrino events.

We employ a χ^2 test to perform three-flavor oscillation analysis. All events are divided into 37 momentum or energy bins (10+5 bins for FC single- and multi-ring e -like, 8+4 bins for FC single- and multi-ring μ -like, 4+4 bins for OD stopping and OD through-going PC, and 1+1 bin for upward stopping and through-going muons). The reconstructed quantities used for momentum binning for the various event classes are: the observed momentum of the charged lepton for FC single-ring e - and μ -like events (P_{lep}), the sum of the energies of the observed rings (reconstructed particles) considering particle mass for FC multi-ring e -like events (E_{tot}), and the sum of visible energies of observed rings for FC multi-ring μ -like and PC events (E_{vis}). Note that the binning of the energy scale differs from that of [5, 12], i.e. events in the multi-GeV energy range are divided more finely in order to obtain better sensitivity to Δm^2 . Each momentum bin is also divided into 10 bins equally spaced between $\cos \Theta = -1$ and $\cos \Theta = +1$ ($-1 < \cos \Theta < 0$ for UP μ events), where $\cos \Theta$ is the cosine of the zenith angle of the reconstructed particle direction. Table III summarizes the number of observed and expected FC, PC and UP μ events for each bin. The total number of bins is 370. The number of events in each bin is compared with expectation and a χ^2 value is calculated according to a Poisson probability distribution defined by the following expression:

$$\chi^2 = \sum_{n=1}^{370} \left[2 \left\{ N_{exp}^n \left(1 + \sum_{i=1}^{45} f_i^n \cdot \epsilon_i \right) - N_{obs}^n \right\} + 2N_{obs}^n \ln \left(\frac{N_{obs}^n}{N_{exp}^n \left(1 + \sum_{i=1}^{45} f_i^n \cdot \epsilon_i \right)} \right) \right] + \sum_{i=1}^{43} \left(\frac{\epsilon_i}{\sigma_i} \right)^2 \quad (6)$$

where

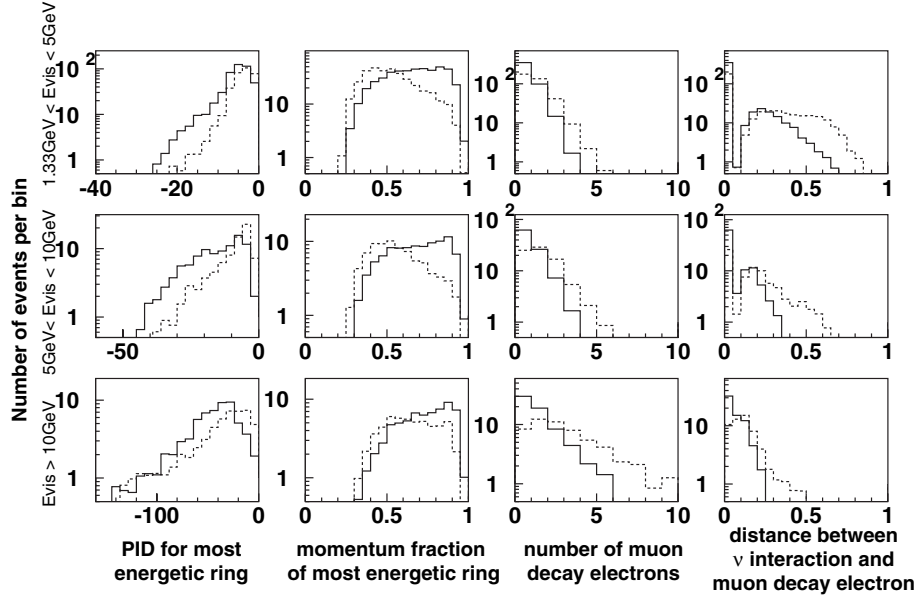


FIG. 2: MC distributions used in the ν_e -enriched likelihood selection for multi-GeV multi-ring e -like events. Plots correspond to $1.33 < E_{vis} < 5$ GeV, $5 < E_{vis} < 10$ GeV, and $E_{vis} > 10$ GeV from top to bottom. From left to right are shown PID likelihood for the most energetic ring (more negative means more electron-like), momentum fraction of the most energetic ring, number of Michel decay electrons, and square root of distance between decay electron and neutrino interaction vertex divided by visible energy of most energetic ring in $(\text{cm/MeV})^{1/2}$. Solid histograms are $\nu_e + \bar{\nu}_e$ CC, dashed are backgrounds (NC + ν_e CC + $\bar{\nu}_\mu$ CC).

N_{obs}^n	Number of observed events in n -th bin
N_{exp}^n	Number of expected events in n -th bin
ϵ_i	i -th systematic error term
f_i^n	Systematic error coefficient
σ_i	1 sigma value of systematic error

N_{exp}^n is calculated using MC events corrected by oscillation probability. Here, systematic uncertainty factors explicitly multiply the N_{exp}^n . We considered 45 systematic error sources, which come from detector calibration, neutrino flux, neutrino interactions and event selection. Most of them are in common with those listed in [5], and additional systematic uncertainties related to backgrounds of the e -like sample and upward-going muons, and sample normalization of e -like events are estimated as listed in Table II. Among 45 errors, only 43 contribute to the χ^2 , because the overall normalization and sample normalization of multi-GeV multi-ring e -like are allowed to be free. f_i^n values are calculated and tabulated in advance for every bin and for every systematic error source. A global scan is carried out on a $(\log_{10}(\Delta m^2), \sin^2 \theta_{23}, \sin^2 \theta_{13})$ grid minimizing χ^2 with respect to 45 systematic error parameters. ϵ_i values are selected in order to minimize the χ^2 value. We used ϵ_i such that the first derivative of χ^2 with respect to ϵ_i is zero ($\frac{\delta \chi^2}{\delta \epsilon_i} = 0$), which can be obtained by solving linear equations [25]. Since this equation has non-linear terms for our χ^2 definition, we use an approximate solution obtained by an iteration method.

A global scan of the oscillation parameter grid assuming normal mass hierarchy results in a minimum χ^2

TABLE II: Sources of systematic errors in addition to those in common with the $\nu_\mu \leftrightarrow \nu_\tau$ oscillation analysis [5]. Non- ν backgrounds in UP μ samples are treated as fitting parameters in this analysis, while they are taken into account by modifying statistical error size in Ref. [5].

	estimated error size (%)
Non- ν background ^a	
upward through-going muons	3.0
upward stopping muons	17
Non- $(\nu_e \text{ CC})$ background ^b	
multi-GeV single-ring e -like	14
multi-GeV multi-ring e -like	20
sample normalization	free
of multi-GeV multi-ring e -like	
OD stopping PC/through-going PC separation	12

^aCosmic ray muon backgrounds are assigned as systematic errors to the most horizontal zenith angle bins ($-0.1 < \cos \Theta < 0$).

^bBackgrounds due to ν_μ CC and all NC interactions.

value of $\chi_{min}^2 = 377.39/368$ DOF at the grid point $(\Delta m^2, \sin^2 \theta_{23}, \sin^2 \theta_{13}) = (2.5 \times 10^{-3} \text{ eV}^2, 0.5, 0.0)$, which is consistent with $\nu_\mu \leftrightarrow \nu_\tau$ two-flavor oscillation. Figure 3 shows the zenith angle distribution of each data sample overlaid with non-oscillated and best-fit expectations. The fitted distributions agree well with data. Figure 4 shows the UP/DOWN asymmetry as a function of particle momentum or total energy. UP/DOWN asymmetry $(\text{UP}-\text{DOWN})/(\text{UP}+\text{DOWN})$ distributions are consistent

with the fitted expectation. No significant excess due to matter effect is seen in the upward-going multi-GeV e -like sample, suggesting no evidence for non-zero θ_{13} . Allowed regions of neutrino oscillation parameters are obtained based on the χ^2 defined in Eq. 6. The 2-dimensional 90 % (99 %) confidence level allowed region is defined to be $\chi^2 = \chi^2_{min} + 4.6$ (9.2) and obtained as shown in Fig. 5. The region corresponding to $\sin^2 \theta_{13} < 0.14$ and $0.37 < \sin^2 \theta_{23} < 0.65$ is allowed at 90% confidence level.

Finally, we tested the inverted mass hierarchy hypothesis. Water Cherenkov detectors, such as Super-K, cannot discriminate between neutrinos and anti-neutrinos on an event-by-event basis. However, mass hierarchy affects the expected number of e -like events. Because of the lower cross section of $\bar{\nu}_e$, an enhancement of the multi-GeV ν_e -rich sample is expected to be suppressed and therefore the constraint on θ_{13} will be weakened for the inverted mass hierarchy case. Allowed regions assuming inverted mass hierarchy are also obtained and shown in Fig. 6. $\chi^2_{min} = 377.31/368$ DOF is obtained at the grid point of $(\Delta m^2, \sin^2 \theta_{23}, \sin^2 \theta_{13}) = (-2.5 \times 10^{-3} \text{eV}^2, 0.525, 0.00625)$. There is little difference in the χ^2_{min} values of the normal and inverted hierarchy cases; therefore both hypotheses are allowed by Super-K data. Figure 7 shows $\chi^2 - \chi^2_{min}$ distributions projected to $\sin^2 \theta_{13}$, in which the minimum χ^2 for each Δm^2 and $\sin^2 \theta_{23}$ are plotted. The $\chi^2 - \chi^2_{min}$ distribution for the inverted hierarchy is flatter and a larger $\sin^2 \theta_{13}$ value is allowed. The constraint on $\sin^2 \theta_{13}$ is weaker for the inverted hierarchy case; $\sin^2 \theta_{13} < 0.27$ and $0.37 < \sin^2 \theta_{23} < 0.69$ are allowed at 90% confidence level.

The present analysis obtained upper limits on θ_{13} which confirms CHOOZ experiment [11] (shown by Fig. 5 and 6) and Palo Verde [26]. These limits are also consistent with the recent result by K2K experiment [27]

giving the upper limit of $\sin^2 \theta_{13} \sim 0.06$ at $\Delta m^2 = 2.8 \times 10^{-3} \text{eV}^2$, assuming $\sin^2 \theta_{23} = 0.5$.

V. CONCLUSION

In summary, a three-flavor oscillation analysis assuming one mass scale dominance ($\Delta m^2_{12} = 0$) was performed with Super-Kamiokande I FC+PC+UP μ combined dataset. A multi-ring e -like sample, selected using a likelihood method, was newly introduced to increase the statistics of electron neutrinos and improve the sensitivity to θ_{13} . The best-fitted parameters for three-flavor oscillation becomes $(\Delta m^2, \sin^2 \theta_{23}, \sin^2 \theta_{13}) = (2.5 \times 10^{-3} \text{eV}^2, 0.5, 0.0)$ and the region of $\sin^2 \theta_{13} < 0.14$ and $0.37 < \sin^2 \theta_{23} < 0.65$ is allowed at 90 % confidence level, assuming normal mass hierarchy. We also tested the inverted mass hierarchy case: a wider region, $\sin^2 \theta_{13} < 0.27$ and $0.37 < \sin^2 \theta_{23} < 0.69$ is allowed at 90 % confidence level. Both mass hierarchy hypotheses agree with our data.

We gratefully acknowledge the cooperation of the Kamioka Mining and Smelting Company. The Super-Kamiokande experiment has been built and operated from funding by the Japanese Ministry of Education, Culture, Sports, Science and Technology, the United States Department of Energy, and the U.S. National Science Foundation. Some of us have been supported by funds from the Korean Research Foundation (BK21) and the Korea Science and Engineering Foundation, the Polish Committee for Scientific Research (grant 1P03B08227), Japan Society for the Promotion of Science, and Research Corporation's Cottrell College Science Award.

-
- [1] R. Becker-Szendy et al., Phys. Rev. **D46**, 3720 (1992).
 - [2] Y. Fukuda et al. (Kamiokande), Phys. Lett. **B335**, 237 (1994).
 - [3] M. Ambrosio et al. (MACRO), Phys. Lett. **B434**, 451 (1998), hep-ex/9807005.
 - [4] M. C. Sanchez et al. (Soudan 2), Phys. Rev. **D68**, 113004 (2003), hep-ex/0307069.
 - [5] Y. Ashie et al. (Super-Kamiokande), Phys. Rev. **D71**, 112005 (2005), hep-ex/0501064.
 - [6] P. Adamson et al. (MINOS) (2005), hep-ex/0512036.
 - [7] M. B. Smy et al. (Super-Kamiokande), Phys. Rev. **D69**, 011104 (2004), hep-ex/0309011.
 - [8] S. N. Ahmed et al. (SNO), Phys. Rev. Lett. **92**, 181301 (2004), nucl-ex/0309004.
 - [9] K. Eguchi et al. (KamLAND), Phys. Rev. Lett. **90**, 021802 (2003), hep-ex/0212021.
 - [10] E. Aliu et al. (K2K), Phys. Rev. Lett. **94**, 081802 (2005), hep-ex/0411038.
 - [11] M. Apollonio et al. (CHOOZ), Phys. Lett. **B466**, 415 (1999), hep-ex/9907037.
 - [12] Y. Ashie et al. (Super-Kamiokande), Phys. Rev. Lett. **93**, 101801 (2004), hep-ex/0404034.
 - [13] O. L. G. Peres and A. Y. Smirnov, Nucl. Phys. **B680**, 479 (2004), hep-ph/0309312.
 - [14] S. P. Mikheyev and A. Y. Smirnov, Yad. Fiz. **42**, 1441 (1985).
 - [15] S. P. Mikheyev and A. Y. Smirnov, Nuov. Cim. **C9**, 17 (1986).
 - [16] L. Wolfenstein, Phys. Rev. **D20**, 2634 (1979).
 - [17] V. D. Barger, K. Whisnant, S. Pakvasa, and R. J. N. Phillips, Phys. Rev. **D22**, 2718 (1980).
 - [18] E. K. Akhmedov, A. Dighe, P. Lipari, and A. Y. Smirnov, Nucl. Phys. **B542**, 3 (1999), hep-ph/9808270.
 - [19] M. Chizhov, M. Maris, and S. T. Petcov (1998), hep-ph/9810501.
 - [20] M. C. Gonzalez-Garcia and M. Maltoni, Eur. Phys. J. **C26**, 417 (2003), hep-ph/0202218.
 - [21] J. Bernabeu, S. Palomares Ruiz, and S. T. Petcov, Nucl. Phys. **B669**, 255 (2003), hep-ph/0305152.
 - [22] Y. Fukuda et al., Nucl. Instrum. Meth. **A501**, 418 (2003).
 - [23] M. Honda, T. Kajita, K. Kasahara, and S. Midorikawa, Phys. Rev. **D70**, 043008 (2004), astro-ph/0404457.

- [24] Y. Hayato, Nucl. Phys. Proc. Suppl. **112**, 171 (2002).
- [25] G. L. Fogli, E. Lisi, A. Marrone, D. Montanino, and A. Palazzo, Phys. Rev. **D66**, 053010 (2002), hep-ph/0206162.
- [26] A. Piepke (Palo Verde), Prog. Part. Nucl. Phys. **48**, 113 (2002).
- [27] S. Yamamoto (K2K) (2006), hep-ex/0603004.

A. Appendix

Table III summarizes the number of observed and expected FC, PC and UP μ events for each bin. The Monte Carlo prediction does not include neutrino oscillations. These binned data are used in the oscillation analysis.

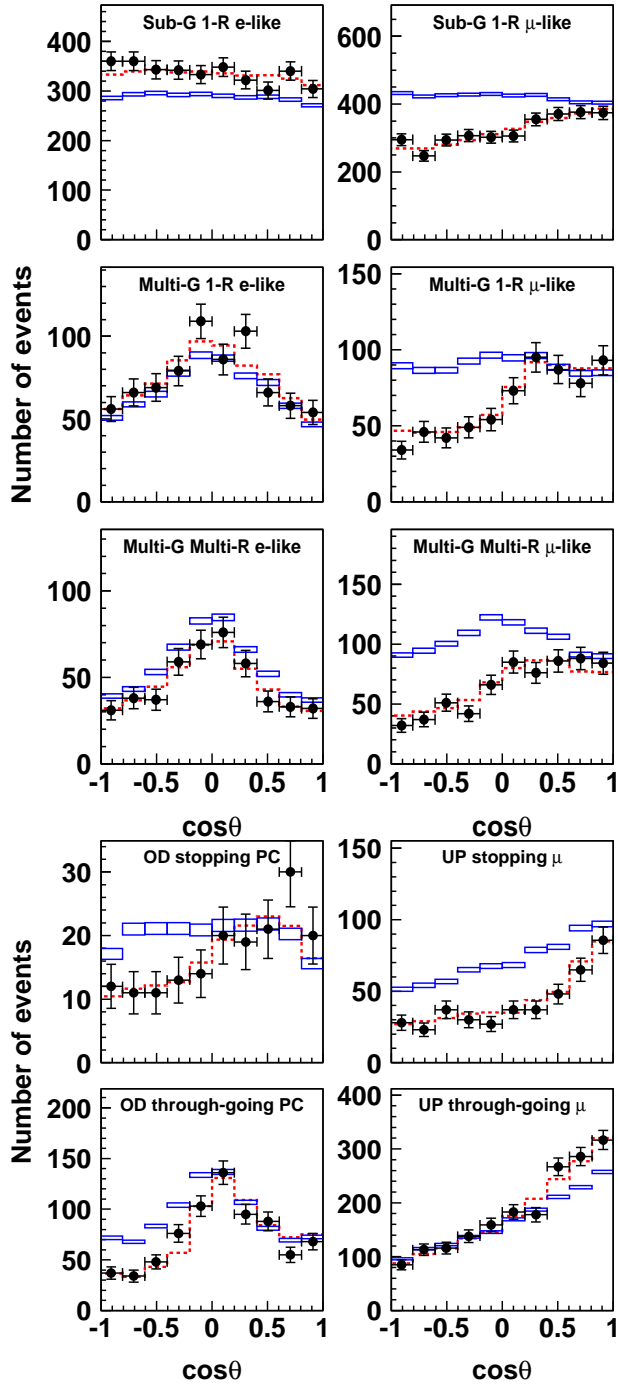


FIG. 3: Zenith angle distributions of FC e -like, μ -like, PC, and $UP\mu$ are shown for data (filled circles with statistical error bars), Monte-Carlo distributions without oscillation (box) and best-fit distributions (dashed). The non-oscillated MC shows the distribution without fitting. The box height shows the statistical error.

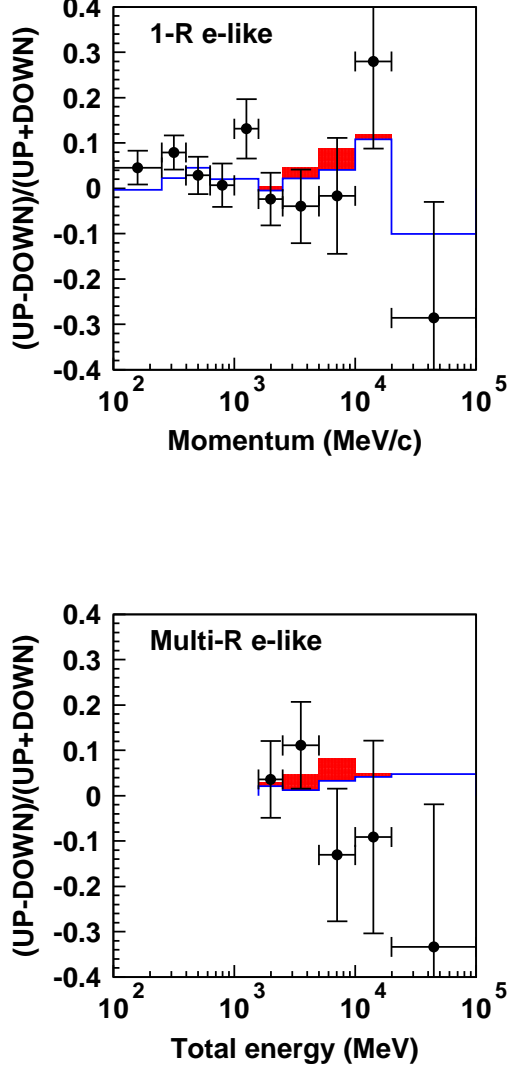


FIG. 4: UP/DOWN asymmetry $(UP-DOWN)/(UP+DOWN)$ as a function of particle momentum for FC single-ring *e*-like events (top) and as a function of total energy for FC multi-ring *e*-like events (bottom). UP (DOWN) refers to the number of events in $-1.0 < \cos \Theta < -0.2$ ($0.2 < \cos \Theta < 1.0$). Filled circles represent data (error bars are statistical), the line represents best-fit distributions under a normal hierarchy assumption, and the filled area on the best-fit line represents the expected excess due to matter effect for $(\Delta m^2, \sin^2 \theta_{23}, \sin^2 \theta_{13}) = (2.5 \times 10^{-3} \text{ eV}^2, 0.5, 0.04)$.

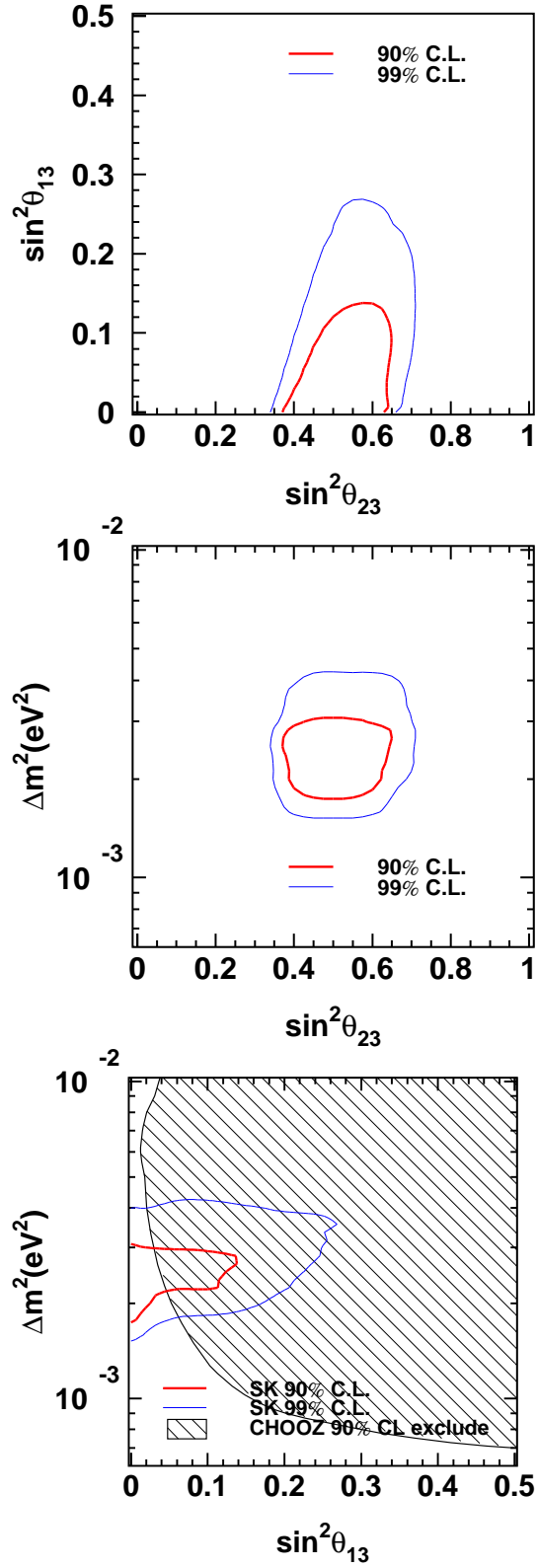


FIG. 5: 90 % (thick line) and 99 % (thin line) confidence level allowed regions are shown in $\sin^2 \theta_{13}$ vs $\sin^2 \theta_{23}$ (top), Δm^2 vs $\sin^2 \theta_{23}$ (middle), and Δm^2 vs $\sin^2 \theta_{13}$ (bottom). Normal mass hierarchy ($\Delta m^2 > 0$) is assumed. The shaded area in the bottom figure shows the region excluded by the CHOOZ reactor neutrino experiment.

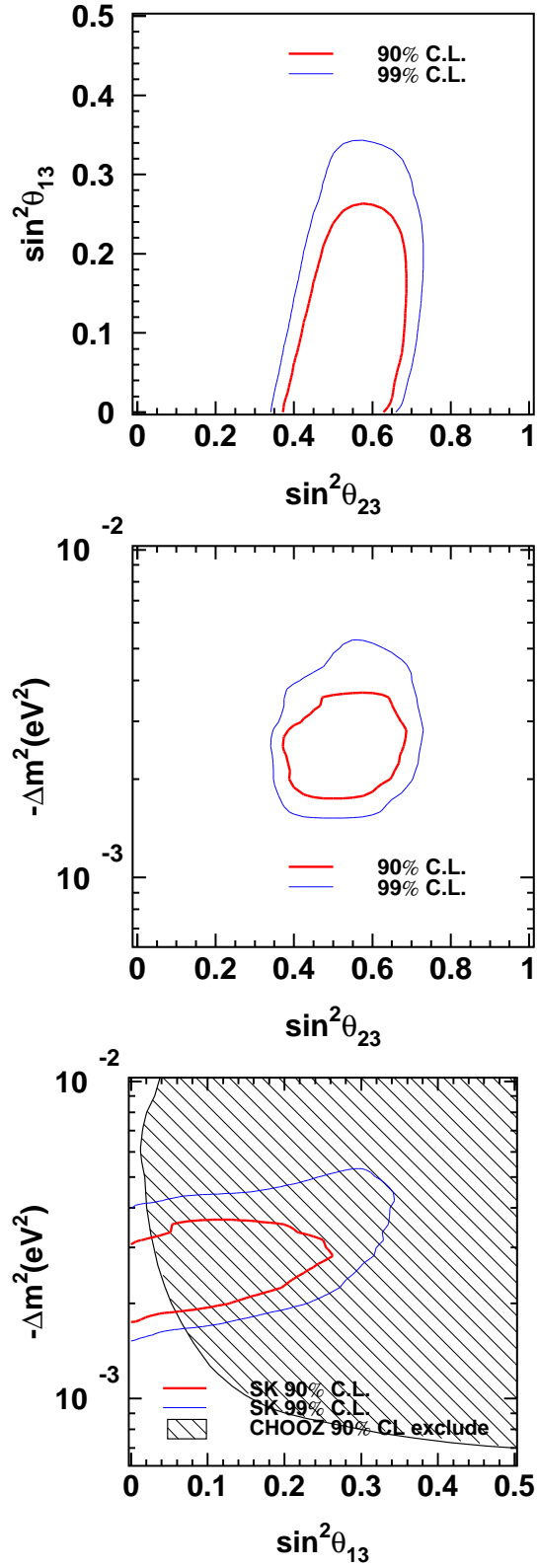


FIG. 6: 90 % (thick line) and 99 % (thin line) confidence level allowed regions assuming inverted mass hierarchy ($\Delta m^2 < 0$), shown in the same orientation as in Fig. 5.

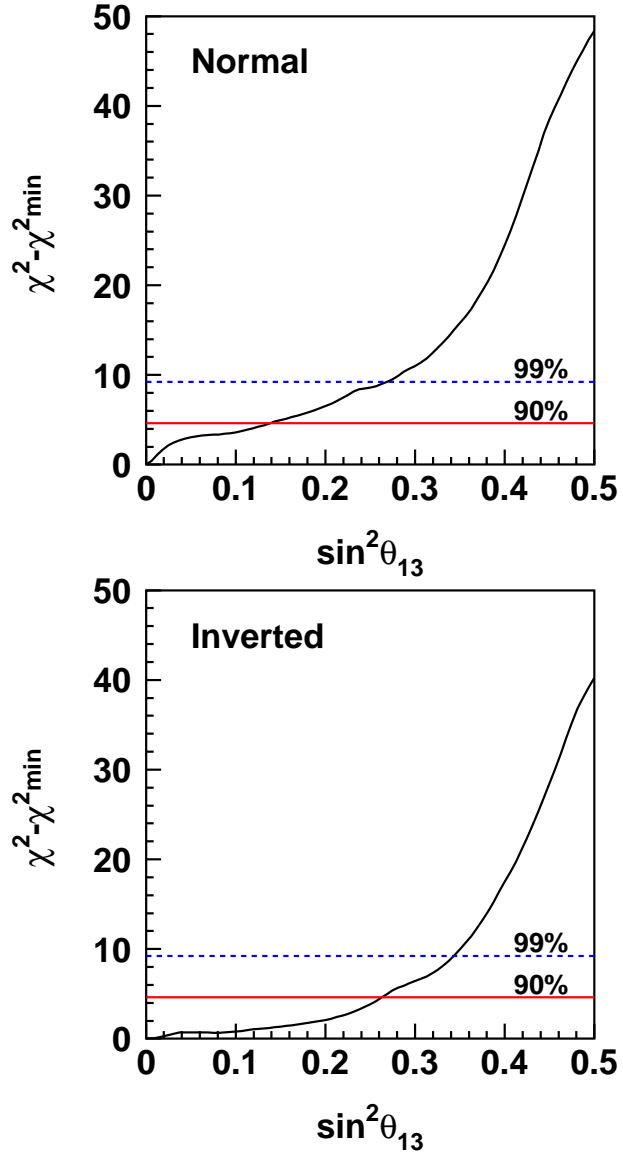


FIG. 7: $\chi^2 - \chi^2_{min}$ as a function of $\sin^2 \theta_{13}$ for normal (top) and inverted (bottom) mass hierarchy assumption. Solid (dashed) lines show 2-dimensional 90 % (99 %) confidence level allowed regions.

FC single-ring e-like										
P_{lep}	I	II	III	IV	V	VI	VII	IIIX	IX	X
1	114(79.3)	95(83.3)	74(81.4)	94(82.0)	88(84.0)	91(79.8)	79(79.5)	74(84.2)	91(81.5)	100(82.9)
2	96(75.6)	93(71.7)	96(73.2)	90(69.4)	89(68.4)	85(68.8)	85(69.5)	74(67.2)	83(71.1)	78(69.7)
3	76(64.2)	80(66.9)	80(65.8)	69(63.6)	72(64.6)	60(64.1)	69(62.4)	71(61.7)	85(59.7)	63(57.5)
4	48(45.4)	57(47.9)	62(50.1)	52(50.9)	60(51.6)	74(51.6)	55(50.8)	58(49.1)	60(46.5)	43(42.5)
5	26(21.7)	35(23.2)	31(25.1)	37(25.8)	24(25.6)	38(25.9)	34(25.0)	24(26.1)	21(23.6)	20(18.5)
6	33(29.3)	35(33.2)	41(34.9)	37(39.7)	46(42.8)	49(43.9)	49(40.7)	32(39.5)	36(32.0)	36(27.3)
7	10(13.8)	20(16.6)	15(18.4)	28(23.5)	36(26.6)	19(24.2)	28(22.0)	24(19.9)	18(17.2)	9(12.4)
8	9(5.27)	5(5.40)	10(7.49)	6(9.42)	14(12.4)	11(11.8)	16(8.38)	8(8.26)	2(5.87)	5(4.18)
9	2(1.47)	4(2.83)	3(2.62)	7(3.73)	7(4.38)	6(4.83)	6(3.38)	1(2.63)	1(1.71)	1(1.63)
10	2(0.86)	2(0.86)	0(1.63)	1(1.26)	6(2.40)	1(2.16)	4(1.68)	1(1.79)	1(1.23)	3(1.26)
FC single-ring μ -like										
P_{lep}	I	II	III	IV	V	VI	VII	IIIX	IX	X
1	36(54.7)	40(53.7)	39(54.4)	37(55.1)	35(55.8)	34(53.8)	35(53.5)	45(53.6)	48(52.6)	46(52.1)
2	86(124)	77(123)	99(123)	86(122)	87(119)	80(120)	91(123)	85(118)	94(116)	76(121)
3	94(119)	60(112)	81(113)	94(116)	87(113)	84(113)	116(113)	119(112)	97(108)	118(105)
4	52(91.1)	48(88.0)	53(90.5)	53(91.0)	68(94.7)	68(91.1)	72(89.6)	81(88.2)	91(84.5)	86(82.9)
5	27(43.4)	22(45.9)	22(44.9)	37(44.5)	25(47.0)	40(47.5)	41(47.9)	41(42.6)	46(44.0)	48(43.6)
6	27(58.8)	35(57.3)	29(59.6)	32(61.6)	35(62.3)	57(63.2)	66(64.4)	69(59.6)	49(55.1)	56(54.0)
7	4(26.1)	10(24.9)	12(23.8)	15(27.3)	16(30.7)	15(28.3)	27(28.6)	16(24.6)	25(25.3)	33(26.8)
8~10	3(4.61)	1(4.21)	1(3.11)	2(3.66)	3(3.36)	1(3.14)	2(3.17)	2(4.19)	4(4.16)	4(4.04)
FC multi-ring e-like										
E_{tot}	I	II	III	IV	V	VI	VII	IIIX	IX	X
b	16(16.9)	18(18.1)	16(21.2)	22(26.9)	26(27.8)	31(27.6)	23(24.0)	19(22.1)	14(16.8)	11(16.0)
c	9(13.4)	12(14.9)	13(18.9)	26(22.4)	21(28.2)	22(28.1)	15(22.2)	11(17.9)	10(14.2)	12(12.8)
d	4(5.77)	3(6.40)	6(8.44)	7(11.3)	12(15.1)	14(16.0)	13(12.4)	3(7.28)	4(6.20)	6(4.77)
e	2(2.17)	4(2.71)	1(2.83)	3(5.05)	5(7.61)	4(8.38)	6(5.19)	2(3.74)	3(1.87)	1(2.07)
f	0(0.89)	1(1.11)	1(1.68)	1(1.75)	5(4.00)	5(4.70)	1(2.33)	1(0.98)	2(0.89)	2(1.21)
FC multi-ring μ -like										
E_{vis}	I	II	III	IV	V	VI	VII	IIIX	IX	X
a	14(27.6)	8(31.2)	20(33.4)	14(33.7)	25(36.1)	16(35.6)	21(34.1)	32(32.9)	29(28.9)	29(29.1)
b	11(33.2)	14(33.6)	16(36.7)	19(39.9)	20(43.9)	33(43.0)	28(40.7)	31(40.7)	30(33.8)	25(32.5)
c	6(22.4)	11(22.8)	11(23.5)	7(27.5)	13(31.6)	20(28.8)	19(28.0)	17(24.8)	23(22.4)	19(20.4)
d~f	1(7.68)	4(6.88)	4(6.73)	2(8.28)	8(10.8)	16(10.9)	8(8.49)	6(7.81)	6(6.29)	11(7.92)
OD stopping PC										
E_{vis}	I	II	III	IV	V	VI	VII	IIIX	IX	X
a	5(4.26)	2(3.53)	2(3.67)	2(4.29)	1(4.98)	5(4.14)	5(4.26)	6(4.14)	9(3.72)	5(3.78)
b	2(4.38)	2(7.23)	3(6.67)	4(5.18)	6(5.81)	2(6.01)	3(6.85)	5(6.76)	9(6.42)	5(4.29)
c	4(4.18)	7(5.61)	3(6.95)	1(6.88)	2(6.02)	5(6.28)	7(5.89)	4(6.57)	4(6.55)	8(4.63)
d~f	1(4.30)	0(4.63)	3(3.81)	6(4.75)	5(4.08)	8(5.16)	4(4.62)	6(4.33)	8(3.56)	2(2.90)
OD through-going PC										
E_{vis}	I	II	III	IV	V	VI	VII	IIIX	IX	X
a	5(9.90)	9(5.69)	10(8.48)	9(11.2)	9(13.5)	9(15.1)	11(13.3)	10(8.53)	10(7.13)	7(9.55)
b	4(13.9)	6(14.0)	10(17.3)	21(22.1)	18(25.2)	18(25.9)	12(19.9)	22(17.9)	11(14.0)	20(14.7)
c	8(18.7)	6(20.9)	12(26.1)	15(32.4)	20(36.9)	48(40.2)	36(34.5)	27(24.1)	11(21.8)	18(22.2)
d~f	20(29.4)	13(27.2)	16(31.5)	31(38.4)	56(58.2)	61(55.6)	36(39.1)	29(30.7)	23(26.5)	23(26.2)
Upward stopping muon										
	28(51.2)	23(54.1)	37(56.7)	30(65.0)	27(67.6)	37(68.2)	37(78.9)	48(81.0)	65(94.0)	85.7(96.9)
Upward through-going muon										
	85(96.1)	113(115)	116(122)	138(137)	159(146)	183(169)	178(187)	267(211)	286(229)	316.6(257)

TABLE III: Summary of the number of observed (MC expected) FC, PC and UP μ events for each bin. Neutrino oscillation is not included in the Monte Carlo prediction. Roman numbers I, II, ... X represent zenith angle regions $-1 < \cos \Theta < -0.8$, $-0.8 < \cos \Theta < -0.6$, ... and $0.8 < \cos \Theta < 1.0$ respectively for FC and PC events, $-1 < \cos \Theta < -0.9$, $-0.9 < \cos \Theta < -0.8$, ... and $0.1 < \cos \Theta < 0.0$ respectively for upward stopping and through-going muon events. The numbers 1 to 5 in the P_{lep} column correspond to the momentum ranges <250 , $250-400$, $400-630$, $630-1000$ and >1000 MeV/c for sub-GeV samples and the numbers 6 to 10 correspond to <2.5 , $2.5-5.0$, $5.0-10$, $10-20$ and >20 GeV/c for multi-GeV samples. The letters a to f in the E_{tot} and E_{vis} columns correspond to energy ranges $0.2-1.33$, $1.33-2.5$, $2.5-5.0$, $5.0-10$, $10-20$, >20 GeV.